Title

IFN-γ activates an immune-like regulatory network in the cardiac vascular endothelium

Authors

Timothy D. Arthur[1,2,⊥], Isaac N. Joshua[3,⊥], Jennifer P. Nguyen[2,4], Agnieszka D'Antonio-Chronowska[5], iPSCORE Consortium*, Kelly A. Frazer[3,6], and Matteo D'Antonio[2]

Affiliations

[1]Biomedical Sciences Graduate Program, University of California, San Diego, La Jolla, 92023

[2]Department of Biomedical Informatics, University of California, San Diego, La Jolla, 92023

[3]Institute of Genomic Medicine, University of California, San Diego, La Jolla, 92023

[4]Bioinformatics and Systems Biology Graduate Program, University of California, San Diego, La Jolla, 92023

[5]Center for Epigenomics, University of California, San Diego, La Jolla, 92023

[6]Department of Pediatrics, University of California, San Diego, La Jolla, 92023

* A full list of Consortium members and their affiliations appears at the end of the manuscript

[⊥] Contributed equally

Abstract

The regulatory mechanisms underlying the response to pro-inflammatory cytokines during myocarditis are poorly understood. Here, we use iPSC-derived cardiovascular progenitor cells (CVPCs) to model the response to interferon gamma (IFN-γ) during myocarditis. We generate RNA-seq and ATAC-seq for four CVPCs that were treated with IFN-γ and compare them with paired untreated controls. Transcriptional differences after treatment show that IFN-γ initiates an innate immune cell-like response in the vascular cardiac endothelium. IFN-γ treatment also shifts the CVPC transcriptome towards the adult coronary artery and aorta profiles and expands the relative endothelial cell population in all four CVPC lines. Analysis of the accessible chromatin shows that IFN-γ is a potent chromatin remodeler and establishes an IRF-STAT immune-cell like regulatory network. Our findings reveal insights into the endothelial-specific protective mechanisms during myocarditis.

Introduction

Myocarditis is an acquired cardiomyopathy due to inflammation of the cardiac muscle. Viral infections[1] and immune checkpoint inhibitor (ICI) treatments in cancer patients[2–4] are common causes of this disease. During infections and ICI treatments, the heart is exposed to a complex cocktail of pro-inflammatory cytokines produced by immune cells. Interferon gamma (IFN–γ), primarily produced by activated $CD4^+$ Th1 cells, stimulates cell type-specific protective and cardiotoxic responses respectively in the endothelial lining of the cardiac vasculature[5–7] and in $CD8^+$ cytotoxic T cells[8]. Studies have demonstrated that IFN–γ stimulates *PD-L1* overexpression in vascular endothelial cells to create a barrier and prevent $CD8^+$ cytotoxic T cell-mediated apoptosis (Figure 1); however, the regulatory mechanism underlying the response to IFN–γ in the vascular endothelium is poorly understood. Utilizing *in vitro* models, such as induced pluripotent stem cell (iPSC)-derived cardiovascular progenitor cells (CVPCs), to understand the impact of IFN–γ on gene expression and regulatory landscapes in cardiac cells could provide important insights into the processes that govern the pathogenesis of myocarditis.

Most efforts to understand myocarditis have relied on mouse models[5,6,8] because obtaining primary cardiac tissues from patients is not possible. CVPCs are a promising model that circumvents the need to use primary cardiac tissues to study drug response and disease molecular mechanisms. The iPSCORE collection consists of 180 CVPCs that were derived from iPSCs from 139 individuals using a lactate selection protocol that only gives rise to cardiac cell types[9]. These CVPCs have extensive molecular characterization, including RNA-seq[10,11], ATAC-seq[12], H3K27 acetylation ChIP-seq[12], ChIP-seq for NKX2-5[13], and Hi-C[14]. In previous studies, we have demonstrated that CVPCs exhibit a fetal-like transcriptomic profile and are composed of several cardiac cell types, including cardiac muscle, smooth muscle, endothelial, and fibroblast cells[10], which enables the characterization of cell type-specific drug responses and contributions to disease.

Here, we use CVPCs from the iPSCORE collection to model the response to IFN-γ in cardiac tissue during myocarditis. We generate RNA-seq and ATAC-seq for four CVPCs derived from iPSCs from four unrelated individuals that were treated with IFN-γ and compare them with paired untreated controls. We show that in all four CVPC lines, IFN-γ treatment shifts the fetal-like CVPC transcriptome towards a more adult coronary artery and aorta-like profile. Cellular deconvolution reveals that IFN-γ treatment expands the relative endothelial cell population. We also show that IFN-γ is a potent chromatin remodeler, and binding sites for IRF and STAT family transcription factors are significantly enriched in the differentially accessible chromatin. Finally, we demonstrate that IFN-γ activates an innate immune cell-like regulatory network in vascular endothelial cells.

Results

IFN-γ stimulates immune cell-independent inflammatory response in cardiac tissue

To examine the effects of IFN-γ on gene expression in cardiac tissues, we performed RNA-seq on four CVPCs that were stimulated with IFN-γ and four paired untreated controls (Table S1). We performed differential expression and identified 2,729 differentially expressed genes (FDR < 0.05), including 1,594 upregulated by IFN-γ stimulation and 1,135 genes that were significantly downregulated (Figure 2a). Despite the absence of immune cell types in CVPCs, many of the upregulated genes were members of the pathogen-responsive JAK-STAT pathway[15] such as *STAT1* (Figure 2b), *IRF1*, *IFI35*, and *ISG15* (Figure 2a, (Table S2). Concordant with previous findings showing that inflammation increases PD-L1 levels in endothelial cells[6], we observed upregulation of *CD274*, which encodes for PD-L1 (Figure 1, Figure 2b). Interestingly, *LEFTY2* and *DANCR*, genes involved in early developmental processes[16,17], are among the genes most downregulated (Figure 2b).

To identify biological processes affected by IFN-γ stimulation, we performed functional enrichment analysis using Enrichr[18] on the 1,594 upregulated genes (Figure 2c, Table S3). In addition to the expected enrichments in immune-related terms, such as response to type 1 interferon ($p = 1.3x10^{-8}$) and regulation of interleukin-12 production ($p = 4.5x10^{-7}$), we observed enrichments in neutrophil gene signatures from different tissues, including lymph nodes, bone marrow, and blood from the *Tabula sapiens* gene set database[19] (Figure 2c). Several gene sets associated with autoimmune disorders (rheumatoid arthritis, multiple sclerosis, complement deficiency, and type 1 diabetes), cancers (kidney cancer and multiple myeloma), and cancer drugs (bortezomib and carfilzomib) were also enriched (Figure 2c).

Taken together, these results show that IFN-γ stimulation in CVPCs upregulates expression of *CD274*, which encodes for PD-L1, consistent with what has been shown to occur in cardiac endothelial cells during inflammation[5,6]. Large expression differences in the JAK-STAT pathway and inflammatory response pathways also occur in the CVPCs notably in the absence of functioning immune cells.

Cardiac endothelial cells drive the IFN-γ stimulated inflammatory response

Given that *CD274* (PD-L1) expression is known to be upregulated in endothelial cells during inflammation[5,6], we hypothesized that upregulation of the inflammatory response pathways may also occur primarily in this cell type. To test this hypothesis, we obtained 180 iPSCORE fetal-like CVPCs, as well as 786 adult cardiovascular RNA-seq samples (left ventricle, atrial appendage, aorta, and coronary artery) from GTEx[20], performed a principal component analysis (PCA), and determined how the IFN-γ treated samples were distinguished from their untreated matched samples in the PCA space (Figure 3a). As expected, PC1 discriminated between fetal-like CVPC and adult tissues, whereas PC2 separated adult cardiomyocyte (atrium and ventricle) from cardiac arterial (aorta and coronary artery) tissues. We observed that, while the four untreated samples from this study clustered with all the other CVPC samples, the treated samples shifted toward the adult cardiac arterial tissues. To confirm that the IFN-γ treated CVPCs were shifting toward the adult cardiac arterial tissues compared to the cardiomyocyte-rich tissues, we collapsed the atrium and ventricle samples into a "CM" group and the aorta and coronary artery samples into an "Arterial" group and calculated the centroid coordinates. We then determined the

Euclidean distances between the 8 CVPCs (treated and control) and the CM and Arterial centroids and performed a paired t-test to examine if IFN-γ treated CVPCs shifted toward the Arterial centroid. Indeed, we observed that the IFN-γ treated CVPCs shifted toward the arterial tissues (p-value = 5.3×10^{-3}), suggesting that IFN-γ stimulation changes the cellular composition of the CVPCs toward a cardiac vascular tissue.

To examine the cellular composition changes in the IFN-γ stimulated CVPCs, we estimated the fractions of the various cell types using CIBERSORT[21] (Figure 3b, Table S4). We showed that the CVPCs were composed of several cell types, including cardiomyocytes, smooth muscle cells, endothelial cells, and fibroblasts; and as expected, the CVPCs were devoid of immune cell types. To test whether IFN-γ treatment influenced the cell type proportions, we performed a paired t-test on the estimated cell type proportions before and after treatment (Figure 3c). Indeed, we found that the fraction of endothelial cells increased significantly in the treated samples ($p = 6.5 \times 10^{-3}$ paired t-test; Figure 3c), indicating that IFN-γ treatment results in an expansion of endothelial cells in culture relative to cardiomyocytes, smooth muscle, and fibroblast proportions. The increased fraction of endothelial cells explains the observed shift of the IFN-γ stimulated fetal-like CVPCs toward adult vascular cardiac tissues (Figure 3a).

Taken together, our findings indicate that cardiac endothelial cells play a protective role during IFN-γ induced inflammation by upregulating PD-L1 and provide new insights that suggest the protective response is also in part due to expansion of the endothelial population (Figure 1, Figure 3b-c). As the other cardiac cell populations remain relatively stable after IFN-γ treatment, these findings suggest that the IFN-γ induced expression of the JAK-STAT and inflammatory response pathways occurs in the cardiac endothelial cells.

IFN-γ establishes an immune regulatory network in cardiac endothelial cells

To profile the epigenomic landscape of cardiac cells treated with IFN-γ, we performed ATAC-seq on the IFN-γ treated CVPCs and their matched controls (Table S1) and identified 119,794 peaks. We performed differential chromatin accessibility analysis on IFN-γ treated CVPCs and their paired controls and identified 3,603 differentially expressed peaks (FDR < 0.05), including 3,576 upregulated by IFN-γ treatment and only 27 that were significantly downregulated (Figure S1, Table S5). These findings suggest that IFN-γ activates a dormant regulatory network while not influencing networks that are active in homeostasis. To functionally characterize upregulated open chromatin, we performed gene set enrichment analysis using GREAT ontology[22], which annotates each peak with the Gene Ontology terms associated with its target genes. We found that overexpressed ATAC-seq peaks activate genes that are associated with interferon signaling, lymphocyte and mononuclear cell proliferation, and macroautophagy (Figure 4a, Table S6).

Transcription factors (TFs) coordinate the expression of genes across the genome, therefore we sought to identify which TFs were binding in IFN-γ upregulated chromatin. We performed TF footprinting analysis[23] using 401 TF motifs[24] in all 119,794 ATAC-seq peaks and evaluated differential TF binding between IFN-γ stimulated and untreated CVPCs (Figure 4b, Table S7). Concordant with the differential gene expression analysis, we observed that TF binding sites (TFBSs) from the IRF (IRF1 mean p-value = 2.5×10^{-173}) and STAT (STAT2 mean p-value = 1×10^{-175}) families had increased binding in the IFN-γ stimulated CVPCs, while developmental TEAD family TFs (TEAD1 mean p-value = 4.7×10^{-98}) and SMAD3

(mean p-value = 3.3×10^{-87}) had increased binding in the untreated CVPCs (Figure 4b). These results suggest that IFN-γ treatment establishes an IRF/STAT-mediated regulatory network to activate the co-expression of inflammatory genes across the genome; and given the concordance with the observed gene expression changes suggests the open chromatin changes are primarily occurring in the endothelial cells.

Since IRF and STAT family TFs are lowly expressed in cardiac tissue in homeostatic conditions (Figure 2a), we hypothesized that IFN-γ upregulated chromatin that is normally inactive. We annotated the 119,794 ATAC-seq peaks with six chromatin states (Promoter, Enhancer, Transcribed regions, Bivalent, Repressed, and Quiescent) in 833 tissues from EpiMap[25]. For each tissue, we tested the enrichment of the 3,576 upregulated peaks in the six chromatin states, using the remaining 116,218 peaks that were not upregulated as background (Figure 4c, Table S8). We observed that upregulated peaks were enriched in quiescent chromatin and transcribed regions and strongly depleted in promoters and enhancers in cardiac tissue (Figure 4c), supporting that IFN-γ opens chromatin that is not accessible in homeostatic cardiac conditions. Additionally, we found that IFN-γ upregulated peaks were most strongly enriched in immune cell type promoters and enhancers (Figure 4c), suggesting that the IFN-γ induced regulatory network in the cardiac endothelium is shared with immune cell types.

Taken together, our results indicate that IFN-γ modulates dramatic chromatin remodeling in the cardiac endothelium by activating an immune cell-like, IRF/STAT-mediated regulatory networks.

Discussion

iPSC-derived tissues are a powerful model for assessing the effects of chemical or environmental stimuli on human tissues that are difficult to obtain. In this study, we demonstrate the utility of using iPSC-derived cardiovascular progenitor cells (CVPCs) to model the cardiac microenvironment in patients with IFN-γ induced myocarditis during viral infections and ICI treatment. We performed RNA-seq and ATAC-seq on four paired IFN-γ treated and control CVPCs to evaluate the transcriptomic and epigenomic changes similar to the effect that occurs when Th1 cells produce inflammatory cytokines after infiltrating cardiac tissue (Figure 1). Despite the absence of immune cell types, IFN-γ stimulated the upregulation of *CD274* (PD-L1) and JAK-STAT-related genes and mounted an immune-like response in cardiac tissue (Figure 2). Additionally, IFN-γ stimulation downregulated key developmental genes (*LEFTY1*, *DANCR*). Indeed, by integrating RNA-seq from 786 adult cardiac samples from four tissues (aorta, atrium, coronary artery, and left ventricle) and 180 CVPCs, we observed that IFN-γ stimulated CVPCs shifted toward the adult aorta and coronary samples relative to their paired controls in the PC space (Figure 3a), indicating that IFN-γ may alter the cell type composition of the cardiac tissue. Cellular deconvolution revealed that IFN-γ stimulation yielded a substantial expansion of endothelial cells (Figure 3b-c). This observation is consistent with previous observations that demonstrate that the vascular endothelium mediates a barrier response to pro-inflammatory cytokines in the heart[5,6]. Recent studies have shown that, in adult cardiac tissues in homeostasis, venous endothelial cells proliferate, while arterial endothelial cells do not[26]. The lack of single-cell data for tissue-specific endothelial cells limited our ability to determine whether the expanding endothelial populations in our study were arterial-like or venous-like. Further experiments are required to determine if the IFN-γ mediates the proliferation of arterial and/or venous endothelium in the adult heart.

Differential chromatin accessibility and TF footprinting analyses revealed that IFN-γ stimulation also upregulated regulatory elements bound by IRF and STAT family TFs that were near genes in immune pathways (Figure 4a-b). We show that regulatory elements upregulated by IFN-γ are inactive in several cardiac tissues, but are active enhancers in dozens of immune cell types, suggesting that the cardiac endothelium adopts an immune-like phenotype during IFN-γ induced inflammation. Noting that fulminant cardiomyopathy only occurs in a small fraction of patients receiving ICI treatment[27], this study provides the framework to evaluate whether there are genetic factors that contribute to its pathology. Future studies can perform quantitative trait loci analyses on gene expression and chromatin accessibility using hundreds of IFN-γ treated CVPCs to identify genetic risk factors associated with cardiac immune-related adverse events in cancer patients. Our results provide biological insights into the protective response to IFN-γ in the cardiac endothelium of patients receiving ICI treatment and demonstrate the utility of using iPSC-derived tissues to model disease phenotypes.

Code Availability

Relevant scripts and notebooks are publicly available at https://github.com/frazer-lab/EndotheliumIFNg.

Data Availability

FASTQ sequencing data for 8 RNA-seq and 8 ATAC-seq samples have been deposited into GSE263611. TOBIAS TF binding predictions, gene expression matrix, signature gene matrix for deconvolution, the ATAC-seq peaks and summits, and the GREAT ontology output results have been deposited in Figshare: (https://figshare.com/projects/Endothelium_IFNg/202329).

Author information

iPSCORE Consortium, University of California, San Diego, La Jolla, CA, 92093, US

Angelo D. Arias, Timothy D. Arthur, Paola Benaglio, Victor Borja, Megan Cook, Matteo D'Antonio, Agnieszka D'Antonio-Chronowska, Christopher DeBoever, Margaret K.R. Donovan, KathyJean Farnam, Kelly A. Frazer, Kyohei Fujita, Melvin Garcia, Olivier Harismendy, David Jakubosky, Kristen Jepsen, Isaac Joshua, He Li, Hiroko Matsui, Naoki Nariai, Jennifer P. Nguyen, Daniel T. O'Connor, Jonathan Okubo, Fengwen Rao, Joaquin Reyna, Lana Ribeiro Aguiar, Bianca Salgado, Nayara Silva, Erin N. Smith, Josh Sohmer, Shawn Yost, William W. Young Greenwald

Contributions

TDA, KAF, and MD conceived the study. TDA, INJ, JPN and iPSCORE consortium members performed the computational analyses. MGR, KAF and MD oversaw the study. ADC and members of the iPSCORE Consortium performed the differentiations and generated molecular data. TDA, INJ, KAF, and MD prepared the manuscript.

Acknowledgments

This work was supported by the National Library Training Grant T15LM011271, the National Institute of Diabetes and Digestive and Kidney Disease (NIDDK) F31DK131867 and P30DK063491, the National Heart, Lung and Blood Institute (NHLBI) F31HL158198 and U01HL107442, and the National Human Genome Research Institute (NHGRI) RM1HG011558. Additional support was also received from a California Institute for Regenerative Medicine grants GC1R-06673-B and EDUC2-08388, and NSF-CMMI division award 1728497.

Declaration of Competing Interests

The authors declare no competing interests.

FIGURES

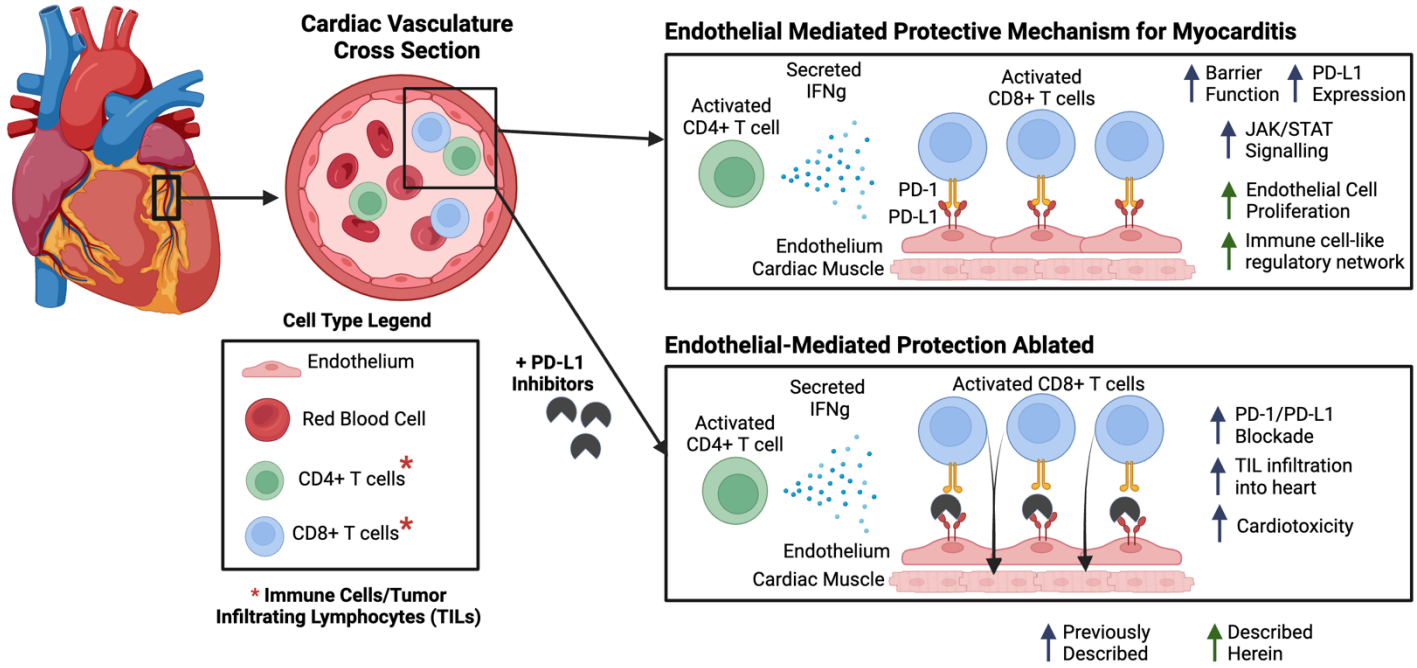

Figure 1. Graphical description of endothelial-mediated protective mechanisms for myocarditis

The most common causes of myocarditis are ICI cancer treatments and viral infections. In both instances, inflammation is caused by IFN-γ secreted by activated immune cells. There are several protective mechanisms that healthy tissues use to evade off-target apoptosis during inflammation. In cardiac tissue, in response to IFN-γ the vascular endothelium is known to function as a barrier by upregulating *CD274* (PD-L1) and JAK/STAT signaling; here, we show that the endothelium also proliferates and activates an immune cell-like regulatory network (top right). In patients receiving PD-L1 inhibitor cancer treatments, the PD-1/PD-L1 pathway is blocked which allows cytotoxic CD8+ T cells to infiltrate the cardiac tissue and cause cardiotoxicity (bottom right).

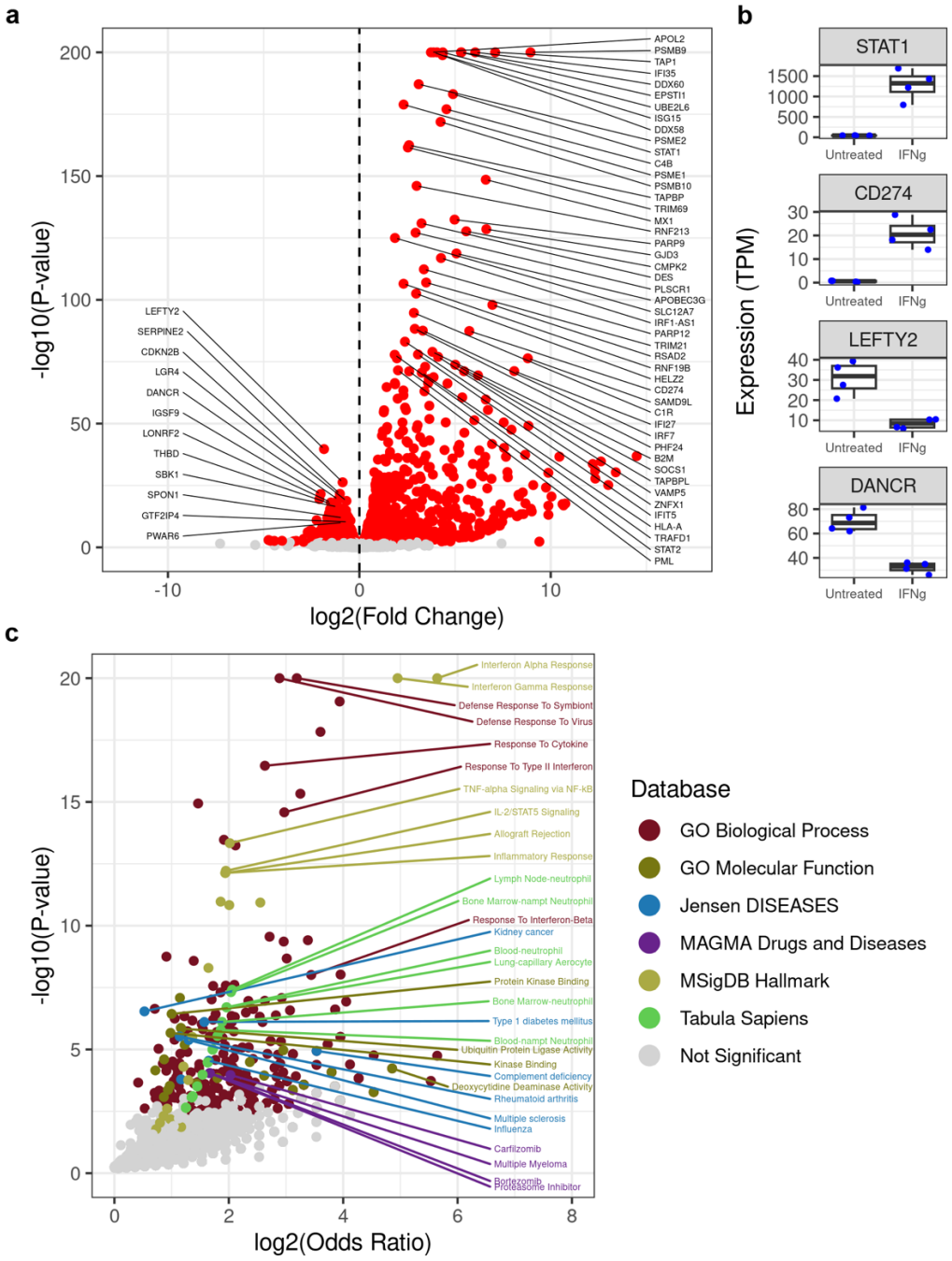

Figure 2. IFN-γ stimulates an immune cell-independent inflammatory response

(A) Volcano plot showing 1,594 upregulated genes and 1,135 downregulated genes upon IFN-γ treatment. The x-axis is the log2 Fold Change, where positive values correspond to genes that are upregulated by IFN-γ and negative values are downregulated genes, the y-axis is the -log10(P-value), and each point represents a gene. The points are colored by significance (FDR < 0.05), where "red" points are significant and "grey" points are not significant.

(B) Box plots showing the expression of four differentially expressed genes; *STAT1* (first row), *CD274* (second row), *LEFTY2* (third row), and *DANCR* (fourth row). The x-axes contain the IFN-γ treatment (Untreated and IFNg-treated), the y-axes contain the expression values (TPM), and the points correspond to the eight CVPC samples.

(C) Volcano plot showing functional enrichment of IFN-γ upregulated genes in six Enrichr databases. The x-axis is the log2(Odds Ratio), the y-axis is the -log10(P-value), and each point represents a gene set. Points are colored by Enrichr database.

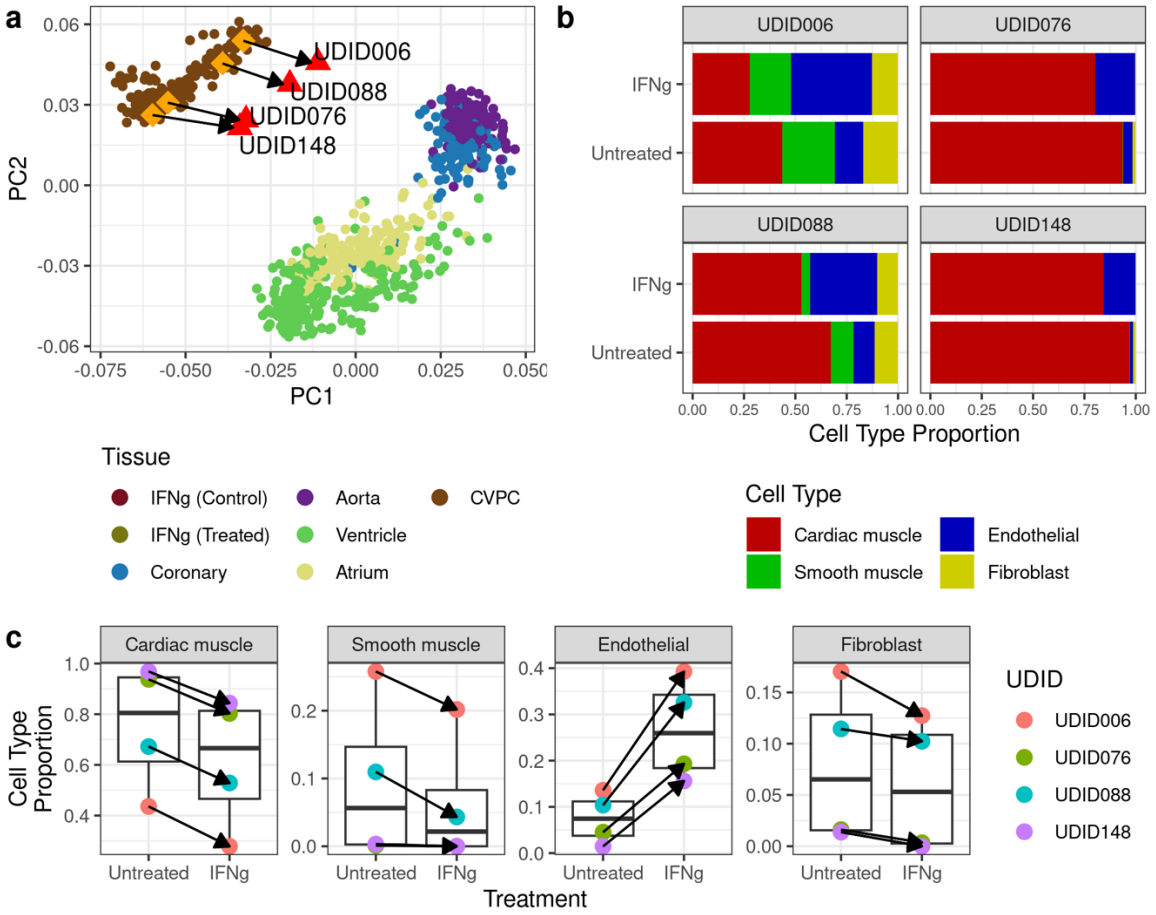

Figure 3. IFN-γ causes the expansion of cardiac endothelial cells

(a) PCA showing the clustering of the 180 original iPSCORE CVPCs[10], 786 GTEx adult cardiac tissues[20], and 8 iPSCORE CVPC samples from this study. PCA was performed on the normalized expression of the 2,729 differentially expressed genes between treated and untreated samples. The 180 original CVPCs and 786 GTEx adult cardiac tissues are represented by circles and are colored by tissue. The untreated CVPC controls from this study are represented by diamonds and colored orange, while the IFN-γ treated CVPCs are represented by triangles and colored red.

(b) Stacked bar plot showing the cardiac cell type estimates of the 8 CVPC samples separated by differentiation. The x-axes describe the estimated proportions of cardiac muscle (red), smooth muscle (green), endothelial (blue), endocardial (pink), and unassigned or "Other" cell types (grey) from CIBERSORT deconvolution, the y-axes are the treatment, either IFN-γ treated (top) or Untreated (bottom), and the four panels correspond to the four CVPC differentiations; UDID006 (top left), UDID076 (top right), UDID088 (bottom left), and UDID148 (bottom right).

(c) Box plots showing the changes in cardiac cell type composition after IFN-γ treatment. The x-axes are the treatment, either Untreated (left) or IFN-γ treated (right), the y-axes are the cell type estimates for cardiac muscle (left), smooth muscle (middle left), endothelial (middle right) and fibroblast (right), and the colored points correspond to the four CVPC differentiations. The arrows indicate the change in cell type proportion after IFN-γ treatment.

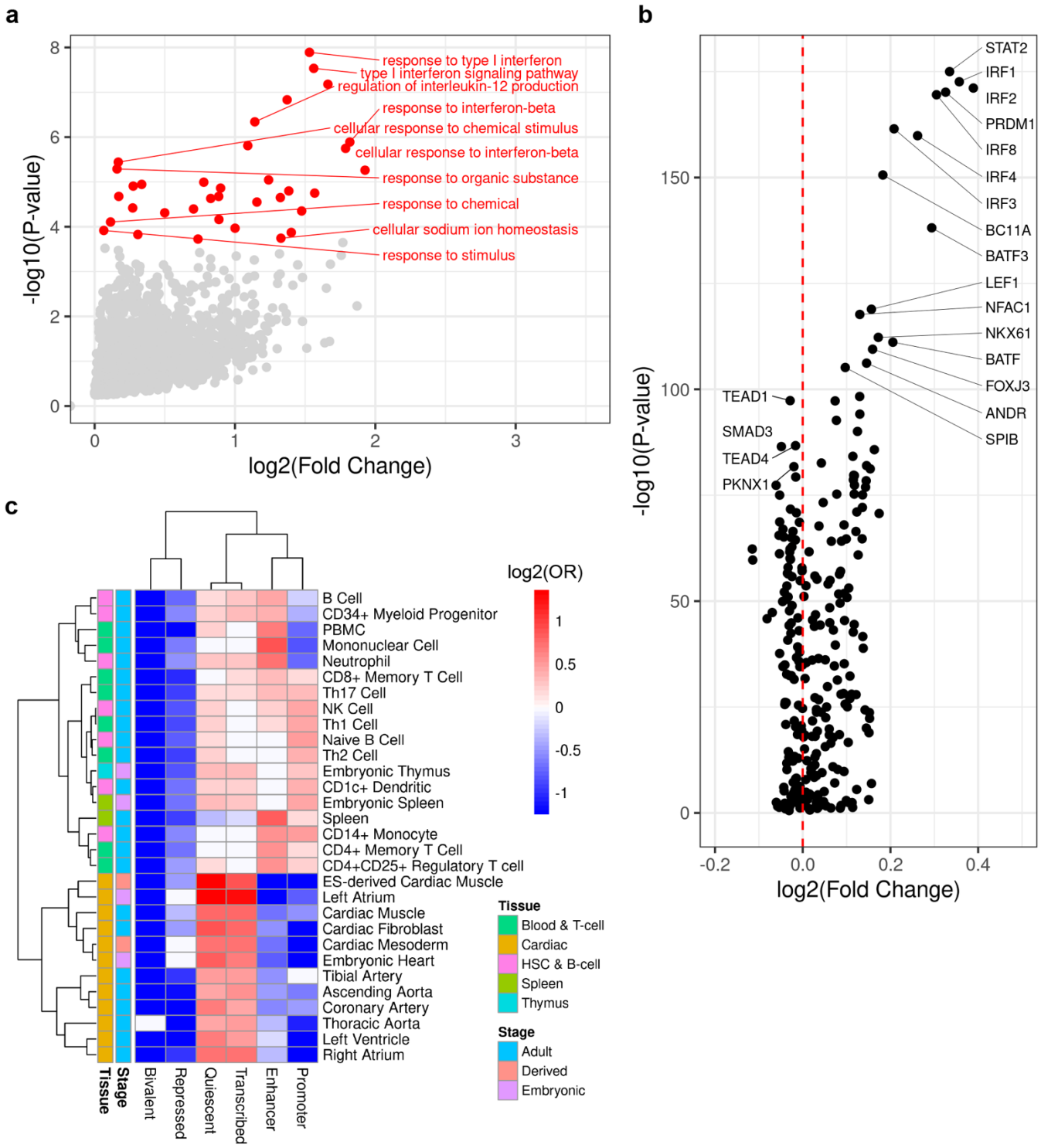

Figure 4. IFN-γ activates an IRF and STAT regulatory network that is shared by immune cell types

(a) Volcano plot showing the enrichment in Gene Ontology gene sets associated with each upregulated peak obtained using GREAT. The x-axis is the log2(Fold Change), the y-axis is the -log10(P-value), and each point represents a gene set. Significant genes are colored red, while non-significant gene sets are colored grey.

(b) Volcano plot showing the enrichment for transcription factor binding footprints in treated compared with untreated samples. The x-axis is the log2(Fold Change), the y-axis is the -log10(P-value), and each point represents a transcription factor. The most significantly enriched and depleted transcription factors are labeled.

(c) Heatmap showing the differential enrichment of IFN-γ upregulated open chromatin in cardiac and immune tissues. The x-axis contains the six collapsed chromatin states, the y-axis contains cardiac and immune tissues from the EpiMap repository, and the cells are filled with the log2(Odds Ratio) enrichments of 3,576 IFN-γ upregulated open chromatin peaks compared to the 116,218 open chromatin peaks not upregulated by IFN-γ treatment. The "Tissue" annotation column indicates whether the corresponding EpiMap tissue is immune (Blood & T-cell, HSC & B-cell, Spleen, Thymus) or cardiac. The "Stage" annotation column indicates whether the corresponding EpiMap tissue is Embryonic, Derived, or Adult.

METHODS

1. CVPC culture and treatment conditions

iPSC lines from four unrelated individuals recruited as part of the iPSCORE project were previously differentiated into CVPCs using small molecules and enriched using metabolic selection with lactate[9,10] (Table S1). The CVPCs were harvested at day 25, which we and others have previously shown represent fetal cardiac cells[28], and cryopreserved at -80° C. The cryopreserved CVPCs (day 25) were then thawed, plated at a density of $2.5x10^5/cm^2$ cells on Matrigel (Corning) coated 6-well plates, and allowed 72 hours for recovery and expansion. On day 28 (three days after thawing), CVPCs were treated with 100 nM human recombinant IFN-γ (ThermoFisher) for 24h. On day 29, control and IFN-γ-treated CVPC samples (eight in total) were harvested.

2. Molecular data generation and sequencing

2.1 RNA-seq

We extracted total RNA from lysed pellets frozen in RLT Plus buffer (collected on day 29) using the Quick-RNA™ MiniPrep Kit (Zymo Research), assessed quality to make sure RNA Integrity number (RIN) was 7.5 or greater, prepared indexed libraries using the Illumina TruSeq stranded mRNA kit and sequenced with 150 bp paired-end reads on an Illumina HiSeq 4000 (mean = 91.4M reads).

2.2 ATAC-seq

ATAC-seq samples were processed as previously described in detail[17]. Briefly, frozen nuclear pellets of $1x10^5$ CVPC were thawed on ice and tagmented in total volume of 25 µl in permeabilization buffer containing digitonin (10 mM Tris-HCl pH 7.5, 10 mM NaCl, 3 mM $MgCl^2$, 0.01% digitonin) and 2.5 µl of Tn5 from Nextera DNA Library Preparation Kit (Illumina) for 45-75min at 37°C in a thermomixer (500 RPM shaking). To eliminate confounding effects due to index hopping, all libraries within a pool were indexed with unique pairs of i7 and i5 barcodes. Libraries were amplified for 12 cycles using NEBNext® High-Fidelity 2X PCR Master Mix (NEB) in total volume of 25µl in the presence of 800 nM of barcoded primers (400nM each) custom synthesized by Integrated DNA Technologies (IDT) and sequenced with 150-bp paired end reads on a HiSeq4000 (mean = 112.9M reads).

3. Data Processing

3.1 RNA-seq

To measure gene expression in the 8 CVPC samples, we obtained raw counts in transcript per million bp (TPM) as previously described[11]. Briefly, FASTQ files were aligned to the hg19 reference human genome using with STAR v.2.7.3[29] and GencodeV.34lift37 with parameters: *--outFilterMultimapNmax 20 --outFilterMismatchNmax 999 --alignIntronMin 20*

--alignIntronMax 1000000 --alignMatesGapMax 1000000. Next, the BAM files were sorted and indexed using sambamba v0.6.7[30], and duplicates were marked using bammarkduplicates from the biobambam software[31]. To quantify gene expression (TPM), we used RSEM version 1.2.20[32] with the following parameters: *rsem-calculate-expression –bam --estimate-rspd --paired-end --forward-prob 0*. RNA-seq sample quality was analyzed with samtools[33] stats, idxstats, and Picard RNA Metrics (Table S1).

3.2 ATAC-seq

The 16 FASTQ files were aligned to the hg19 reference genome with STAR using the following parameters; *--outFilterMultimapNmax 20, -- outFilterMismatchNmax 999, --outFilterMismatchNoverLmax 0.04, --seedSearchStartLmax 20, -- outFilterScoreMinOverLread 0.1, outFilterMatchNminOverLread 0.1.* Sample mate coordinates were filled using samtools fixmate and duplicates were marked using samtools markdup[33]. We then removed poorly mapped reads, fragments < 38 bp, fragments > 2,000 bp, and reads that did not map to autosomal or sex chromosomes with samtools view[33]. Finally, we removed reads in the blacklisted regions (https://mitra.stanford.edu/kundaje/akundaje/release/blacklists/hg19-human/wgEncodeHg19ConsensusSignalArtifactRegions.bed.gz) using bedtools intersect[34] with the *v* parameter.

4. Analysis

4.1 RNA-seq

4.1.1 Differential Gene Expression

The standard DESeq2 (version 1.34.0)[35] workflow for identifying differentially expressed genes was followed. Briefly, the counts and associated metadata for all 8 RNA-seq samples were loaded into a DESeq2 object using the *DESeqDataSetFromMatrix* function. To account for cell type differences between samples, the design was specified as ~ UDID + treatment and the *DESeq* function was applied to identify genes that are differentially expressed (Benjamini-Hochberg's Adjusted P-value < 0.05) by IFN-γ treatment.

4.1.2 Functional Enrichment Analysis

The 1,594 upregulated genes DESeq2 were used as input into Enrichr[18] and functional enrichment analysis was performed with standard parameters on all libraries cumulatively containing >420k gene sets. For plot legibility, the following gene set libraries were prioritized; Jensen DISEASES, MAGMA Drugs and Diseases, Tabula Sapiens, GO Biological Process 2023, GO Molecular Function 2023, MSigDB Hallmark 2020, and IDG Drug Targets 2022.

4.1.3 Integrated PCA

We obtained gene expression (TPM) values for 180 iPSCORE CVPC samples, 207 adult left ventricle, 187 atrial appendage, 215 aorta, and 117 coronary artery samples from GTEx from our previous studies (10.6084/m9.figshare.16920658)[11,20], combined these with the TPM values for the IFN-γ-treated and control samples, and performed quantile normalization using

the *normalize.quantiles* function from the preprocessCore package and qnorm functions in R, and obtained mean expression = 0 and standard deviation = 1 for each gene. We extracted the normalized expression levels of the 2,729 differentially expressed genes (1,594 upregulated and 1,135 downregulated) and performed PCA using the prcomp function in R.

4.1.4 Cellular Deconvolution

Cell type proportions were computed with digital deconvolution using CIBERSORT[21]. Deconvolution of bulk cell type composition requires identifying marker genes by their associated expression levels to assign predictive cell-type classes based on one of several cardiac cell populations. The marker genes we used as input into CIBERSORT were identified using the published scRNA-seq data from the *Tabula sapiens* collection[19]. We obtained the scRNA-seq from the *Tabula sapiens* heart dataset (https://figshare.com/articles/dataset/Tabula_Sapiens_release_1_0/14267219) which is composed of 11,505 cells annotated with six cell types (cardiac muscle, smooth muscle, endothelial, fibroblasts, macrophages, and hepatocytes). We loaded the dataset into Seurat (version 4.3.0)[36] and removed cells annotated as "macrophages" and "hepatocytes" because the CVPC differentiation can only give rise to cardiac lineage cell types. After filtering, we renormalized, rescaled, and reclustered the cells at resolution = 0.08, using Seurat. We annotated 5 of the 6 resulting clusters, using original *Tabula sapiens* annotations (two clusters mapped to cardiac muscle, one cluster mapped to smooth muscle, endothelial, and fibroblast each). The unassigned cluster exhibited increased expression of markers for antigen presenting cells and was composed of < 60 cells, therefore we removed it. We then ran the Seurat FindAllMarkers function using the parameters *logfc.threshold = 0.1, only.pos = TRUE,* and *min.pct = 0.2* to obtain marker genes and classify cardiac cell types belonging to the four remaining cardiac cell types in *Tabula sapiens*. We removed genes that were not expressed in the CVPCs, then selected the top 250 marker genes (Adjusted p-value < 0.05) for each cell type, then removed genes that were markers for more than one cell type and selected the top 100 marker genes from the remaining genes. We then used the AverageExpression function in Seurat, which generated average expression levels for each cell type. Finally, CIBERSORT was performed with quantile normalization = FALSE on the 8 paired treated and control CVPC sample gene expression matrices (TPM) to yield the estimates for the four cell types.

4.2 ATAC-seq

4.2.1 MACS2 Peak Calling

Narrow peaks were called using MACS2[37] on each of the 8 BAM files individually, using the following parameters; -f BAMPE -g hs --nomodel --shift -100 --extsize 200 --call-summits –q 0.01, which resulted in an average of 77,643 ± 33,040 peaks per sample. We merged the peak bed files from the 8 ATAC-seq samples, then removed peaks that were only present in one sample which resulted in 119,794 reference peaks. For each sample, we counted the number of reads in the reference peaks using featureCounts[38].

4.2.2 Differential Chromatin Accessibility

The standard DESeq2 (version 1.34.0)[35] workflow for identifying differentially accessible peaks was followed. Briefly, the counts and associated metadata for all 8 ATAC-seq samples were loaded into a DESeq2 object using the *DESeqDataSetFromMatrix* function. To account for cell type differences between samples, the design was specified as ~ UDID + treatment and the *DESeq* function was applied to identify ATAC-seq peaks that are differentially accessible (Benjamini-Hochberg's Adjusted P-value < 0.05) by IFN-γ treatment.

4.2.3 GREAT functional enrichment of upregulated peaks

The 3,576 upregulated peaks from DESeq2 were used as input, and all 119,794 peaks as background, to perform functional enrichment analysis on Gene Ontology Biological Process, Molecular Function, and Cellular Component gene sets using GREAT[22].

4.2.4 Transcription Factor Binding Site Predictions

We used TOBIAS[23] to predict binding motifs and map potential transcription factor occupancy sites across our peaks to profile chromatin accessibility after IFN-γ stimulation. We ran TOBIAS ATACorrect on the 8 BAM files to correct for cut site biases introduced by the Tn5 transposase within the 119,794 ATAC-seq peaks using the following parameters: --genome hg19 fasta and – blacklist hg19blacklist.v2.bed (from https://mitra.stanford.edu/kundaje/akundaje/release/blacklists/hg19-human/wgEncodeHg19ConsensusSignalArtifactRegions.bed.gz). Next, we calculated footprint scores with TOBIAS ScoreBigWig, using the BED file containing the coordinates of all the 119,794 ATAC-seq peaks. Finally, to calculate differential transcription factor binding between control and IFN-γ treated CVPCs, we ran TOBIAS BINDetect on each CVPC (UDID) using position weight matrices (PWM) for 401 HOCOMOCO V.11[24] transcription factors, using the following parameters: --motif *HOCOMOCO PWM file* –signals *untreatedUDID.bw treatedUDID.bw*. For plot legibility, we plotted the average fold change and p-value across the four UDIDs for 265 TFs with motif quality ("A" or "B").

4.2.5 Differential Chromatin State Enrichment

We obtained 18 ChromHMM chromatin states from 833 tissues from the Epimap Repository[25] (https://personal.broadinstitute.org/cboix/epimap/ChromHMM/observed_aux_18_hg19/CALLS/). For all 833 tissues, we collapsed the 18 chromatin states into 6 states, including Promoter ("TssA", "TssFlnk", "TssFlnkU", "TssFlnkD"), Enhancer ("EnhA1", "EnhA2", "EnhG1", "EnhG2", "EnhWk"), Transcribed ("Tx", "TxWk"), Bivalent ("TssBiv", "EnhBiv"), Repressed ("ReprPC", "ReprPCWk", "ZNF/Rpts", "Het"), and Quiescent ("Quies"). We used the coordinates of the maximum summit of each peak to annotate all 119,794 ATAC-seq peaks with the 6 collapsed chromatin states from all 833 EpiMap tissues, using bedtools intersect[34]. For each tissue, we performed Fisher's Exact tests to test the differential enrichment of 3,576 IFN-γ upregulated ATAC-seq peaks in the six chromatin states using the 116,218 ATAC-seq not upregulated by IFN-γ treatment as background.

SUPPLEMENTAL TABLE LEGENDS

Table S1: Study Metadata

Sheet 1: Subject Metadata: This table contains information on the iPSCORE subject whose data was analyzed in this study. The columns describe the **iPSCORE_ID** and the **Subject_UUID** which is a universal unique identifier, the iPSCORE **Family_ID**, the **Sex** of the donor, and the **Age_at_Enrollment**.

Sheet 2: RNA-seq Sample Metadata: This table contains information and quality metrics of the RNA-seq samples analyzed in this study. The columns describe the **UDID** the CVPC unique differentiation identifier, **Treatment** either untreated "CONTROL" or "IFNg" treated, **Sample_UUID** the sample universal unique identifier, the **iPSCORE_ID** and **Subject_UUID** of the donor, and the quality control metrics of the samples, including the number of **Total Reads**, **Duplicates**, **Mapped** reads, and **Properly Paired** reads.

Sheet 3: ATAC-seq Sample Metadata: This table contains information and quality metrics of the RNA-seq samples analyzed in this study. The columns describe the **UDID** the CVPC unique differentiation identifier, **Treatment** either untreated "CONTROL" or "IFNg" treated, **Sample_UUID** the sample universal unique identifier, the **iPSCORE_ID** and **Subject_UUID** of the donor, and the quality control metrics of the samples, including the number of **Total Reads**, **Mapped** reads, and **Properly Paired** reads.

Table S2: Differential Gene Expression

This table contains the output from differential gene expression analysis performed using the DESeq2 R package. The columns include the **Gene Name** and **Gene ID** from Gencode.v34lift37, and the standard output of DESeq2, including **baseMean**, **log2FoldChange**, **lfcSE** (standard error of the log2 fold change), **stat** (the Wald statistic), **p-value**, and the Benjamini Hochberg **Adjusted p-value**. Non-significant (adjusted p-value > 0.05), IFN-γ upregulated (adjusted p-value < 0.05 & log2FoldChange > 0) and IFN-γ downregulated (adjusted p-value < 0.05 & log2FoldChange < 0) genes are reported.

Table S3: Enrichr Gene Set Enrichment Results

This table contains the output for the gene set enrichment analysis performed using the Enrichr R package. The columns describe the **Database** in Enrichr, the **Term** for the gene set, the **Number of Upregulated Genes in the Term**, the **Total Number of Genes in the Term**, the nominal **P-value**, Benjamini Hochberg **Adjusted P-value**, and the **Odds Ratio**.

Table S4: CIBERSORT Cell Type Estimates

This table includes the CIBERSORT estimated cell type proportions of CVPC RNA-seq before and after IFN-γ treatment. The columns describe the **UDID** (unique differentiation identifier) for the CVPC line, **Treatment** (Control or IFNg), and the CIBERSORT relative estimates for **Cardiac Muscle, Smooth Muscle**, **Endothelial**, and **Fibroblast**.

Table S5: Differential Chromatin Accessibility

This table contains the output from differential chromatin accessibility analysis performed using the DESeq2 R package. The columns include the **Peak ID** which describes the hg19 coordinates of the peak, and the standard output of DESeq2, including **baseMean**, **log2FoldChange**, **lfcSE** (standard error of the log2 fold change), **stat** (the Wald statistic), **p-value**, and the Benjamini Hochberg **Adjusted p-value**. Non-significant (adjusted p-value > 0.05), IFN-γ upregulated (adjusted p-value < 0.05 & log2FoldChange > 0) and IFN-γ downregulated (adjusted p-value < 0.05 & log2FoldChange < 0) peaks are reported.

Table S6: ATAC-seq Gene Set Enrichment with GREAT

This table contains the results from the GREAT Ontology ATAC-seq peak enrichment analysis. The columns include **Database** (Molecular Function, Cellular Component or Biological Process), the gene set or **Term** and the **GO ID**, the **FoldEnrichment, Pvalue**, and the the Benjamini Hochberg Adjusted p-value (**FDR**) value.

Table S7: Differentially Transcription Factor Binding with TOBIAS

This table contains the results from the TOBIAS differential transcription factor binding analysis. The columns describe the **UDID** (unique differentiation identifier) for the CVPC line, the **MotifID** from HOCOMOCO database, and the **FoldChange** and **Pvalue** computed by TOBIAS.

Table S8: Chromatin State Enrichment

This table contains the results from differential chromatin state enrichment of IFN-γ upregulated ATAC-seq peaks in 833 EpiMap tissues. The columns contain the **BSS ID** and **EpiMap Tissue Name**, the tested **Collapsed Chromatin State**, the Odds Ratio (**OR**), the **Pvalue** and Benjamini Hochberg Adjusted P-value (**Padj**) from the Fisher's Exact test, whether or not the corresponding tissue was **Plotted** in Figure 4c. Additional information about the tissues can be obtained from the EpiMap metadata file (https://personal.broadinstitute.org/cboix/epimap/metadata/Imputation_Metadata.xlsx).

REFERENCES

1. Mantri, M., Hinchman, M.M., McKellar, D.W., Wang, M.F.Z., Cross, S.T., Parker, J.S.L., and De Vlaminck, I. (2022). Spatiotemporal transcriptomics reveals pathogenesis of viral myocarditis. Nat Cardiovasc Res *1*, 946–960. 10.1038/s44161-022-00138-1.

2. Johnson, D.B., Balko, J.M., Compton, M.L., Chalkias, S., Gorham, J., Xu, Y., Hicks, M., Puzanov, I., Alexander, M.R., Bloomer, T.L., et al. (2016). Fulminant Myocarditis with Combination Immune Checkpoint Blockade. N Engl J Med *375*, 1749–1755. 10.1056/NEJMoa1609214.

3. Ball, S., Ghosh, R.K., Wongsaengsak, S., Bandyopadhyay, D., Ghosh, G.C., Aronow, W.S., Fonarow, G.C., Lenihan, D.J., and Bhatt, D.L. (2019). Cardiovascular Toxicities of Immune Checkpoint Inhibitors: JACC Review Topic of the Week. J Am Coll Cardiol *74*, 1714–1727. 10.1016/j.jacc.2019.07.079.

4. Raskov, H., Orhan, A., Christensen, J.P., and Gögenur, I. (2021). Cytotoxic CD8+ T cells in cancer and cancer immunotherapy. Br J Cancer *124*, 359–367. 10.1038/s41416-020-01048-4.

5. Tay, W.T., Fang, Y.-H., Beh, S.T., Liu, Y.-W., Hsu, L.-W., Yen, C.-J., and Liu, P.-Y. (2020). Programmed Cell Death-1: Programmed Cell Death-Ligand 1 Interaction Protects Human Cardiomyocytes Against T-Cell Mediated Inflammation and Apoptosis Response In Vitro. Int J Mol Sci *21*, 2399. 10.3390/ijms21072399.

6. Rodig, N., Ryan, T., Allen, J.A., Pang, H., Grabie, N., Chernova, T., Greenfield, E.A., Liang, S.C., Sharpe, A.H., Lichtman, A.H., et al. (2003). Endothelial expression of PD-L1 and PD-L2 down-regulates CD8+ T cell activation and cytolysis. Eur J Immunol *33*, 3117–3126. 10.1002/eji.200324270.

7. Garcia-Diaz, A., Shin, D.S., Moreno, B.H., Saco, J., Escuin-Ordinas, H., Rodriguez, G.A., Zaretsky, J.M., Sun, L., Hugo, W., Wang, X., et al. (2017). Interferon Receptor Signaling Pathways Regulating PD-L1 and PD-L2 Expression. Cell Rep *19*, 1189–1201. 10.1016/j.celrep.2017.04.031.

8. Grabie, N., Gotsman, I., DaCosta, R., Pang, H., Stavrakis, G., Butte, M.J., Keir, M.E., Freeman, G.J., Sharpe, A.H., and Lichtman, A.H. (2007). Endothelial programmed death-1 ligand 1 (PD-L1) regulates CD8+ T-cell mediated injury in the heart. Circulation *116*, 2062–2071. 10.1161/CIRCULATIONAHA.107.709360.

9. D'Antonio-Chronowska, A., D'Antonio, M., and Frazer, K. (2020). In vitro Differentiation of Human iPSC-derived Cardiovascular Progenitor Cells (iPSC-CVPCs). BIO-PROTOCOL *10*. 10.21769/BioProtoc.3755.

10. D'Antonio-Chronowska, A., Donovan, M.K.R., Young Greenwald, W.W., Nguyen, J.P., Fujita, K., Hashem, S., Matsui, H., Soncin, F., Parast, M., Ward, M.C., et al. (2019). Association of Human iPSC Gene Signatures and X Chromosome Dosage with Two Distinct Cardiac Differentiation Trajectories. Stem Cell Reports *13*, 924–938. 10.1016/j.stemcr.2019.09.011.

11. D'Antonio, M., Nguyen, J.P., Arthur, T.D., iPSCORE Consortium, Arias, A.D., Arthur, T.D., Benaglio, P., Berggren, W.T., Borja, V., Belmonte, J.C.I., et al. (2023). Fine mapping spatiotemporal mechanisms of genetic variants underlying cardiac traits and disease. Nat Commun *14*, 1132. 10.1038/s41467-023-36638-2.

12. Arthur, T.D., Nguyen, J.P., D'Antonio-Chronowska, A., Jaureguy, J., Silva, N., Henson, B., iPSCORE Consortium, Panopoulos, A.D., Belmonte, J.C.I., D'Antonio, M., et al. (2024). Multi-omic QTL mapping in early developmental tissues reveals phenotypic and temporal complexity of regulatory variants underlying GWAS loci. Preprint, 10.1101/2024.04.10.588874 10.1101/2024.04.10.588874.

13. Benaglio, P., D'Antonio-Chronowska, A., Ma, W., Yang, F., Young Greenwald, W.W., Donovan, M.K.R., DeBoever, C., Li, H., Drees, F., Singhal, S., et al. (2019). Allele-specific NKX2-5 binding underlies multiple genetic associations with human electrocardiographic traits. Nat Genet *51*, 1506–1517. 10.1038/s41588-019-0499-3.

14. Greenwald, W.W., Li, H., Benaglio, P., Jakubosky, D., Matsui, H., Schmitt, A., Selvaraj, S., D'Antonio, M., D'Antonio-Chronowska, A., Smith, E.N., et al. (2019). Subtle changes in chromatin loop contact propensity are associated with differential gene regulation and expression. Nat Commun *10*, 1054. 10.1038/s41467-019-08940-5.

15. Hu, X., Li, J., Fu, M., Zhao, X., and Wang, W. (2021). The JAK/STAT signaling pathway: from bench to clinic. Signal Transduct Target Ther *6*, 402. 10.1038/s41392-021-00791-1.

16. Lau, K.X., Mason, E.A., Kie, J., De Souza, D.P., Kloehn, J., Tull, D., McConville, M.J., Keniry, A., Beck, T., Blewitt, M.E., et al. (2020). Unique properties of a subset of human pluripotent stem cells with high capacity for self-renewal. Nat Commun *11*, 2420. 10.1038/s41467-020-16214-8.

17. Arthur, T.D., Nguyen, J.P., D'Antonio-Chronowska, A., Matsui, H., Silva, N.S., Joshua, I.N., iPSCORE Consortium, Aguiar, L.R., Arias, A.D., Benaglio, P., et al. (2024). Complex regulatory networks influence pluripotent cell state transitions in human iPSCs. Nat Commun *15*, 1664. 10.1038/s41467-024-45506-6.

18. Kuleshov, M.V., Jones, M.R., Rouillard, A.D., Fernandez, N.F., Duan, Q., Wang, Z., Koplev, S., Jenkins, S.L., Jagodnik, K.M., Lachmann, A., et al. (2016). Enrichr: a comprehensive gene set enrichment analysis web server 2016 update. Nucleic Acids Res *44*, W90-97. 10.1093/nar/gkw377.

19. Tabula Sapiens Consortium*, Jones, R.C., Karkanias, J., Krasnow, M.A., Pisco, A.O., Quake, S.R., Salzman, J., Yosef, N., Bulthaup, B., Brown, P., et al. (2022). The Tabula Sapiens: A multiple-organ, single-cell transcriptomic atlas of humans. Science *376*, eabl4896. 10.1126/science.abl4896.

20. The GTEx Consortium, Aguet, F., Anand, S., Ardlie, K.G., Gabriel, S., Getz, G.A., Graubert, A., Hadley, K., Handsaker, R.E., Huang, K.H., et al. (2020). The GTEx Consortium atlas of genetic regulatory effects across human tissues. Science *369*, 1318–1330. 10.1126/science.aaz1776.

21. Chen, B., Khodadoust, M.S., Liu, C.L., Newman, A.M., and Alizadeh, A.A. (2018). Profiling Tumor Infiltrating Immune Cells with CIBERSORT. Methods Mol Biol *1711*, 243–259. 10.1007/978-1-4939-7493-1_12.

22. McLean, C.Y., Bristor, D., Hiller, M., Clarke, S.L., Schaar, B.T., Lowe, C.B., Wenger, A.M., and Bejerano, G. (2010). GREAT improves functional interpretation of cis-regulatory regions. Nat Biotechnol *28*, 495–501. 10.1038/nbt.1630.

23. Bentsen, M., Goymann, P., Schultheis, H., Klee, K., Petrova, A., Wiegandt, R., Fust, A., Preussner, J., Kuenne, C., Braun, T., et al. (2020). ATAC-seq footprinting unravels kinetics of transcription factor binding during zygotic genome activation. Nat Commun *11*, 4267. 10.1038/s41467-020-18035-1.

24. Kulakovskiy, I.V., Vorontsov, I.E., Yevshin, I.S., Sharipov, R.N., Fedorova, A.D., Rumynskiy, E.I., Medvedeva, Y.A., Magana-Mora, A., Bajic, V.B., Papatsenko, D.A., et al. (2018). HOCOMOCO: towards a complete collection of transcription factor binding models for human and mouse via large-scale ChIP-Seq analysis. Nucleic Acids Res *46*, D252–D259. 10.1093/nar/gkx1106.

25. Boix, C.A., James, B.T., Park, Y.P., Meuleman, W., and Kellis, M. (2021). Regulatory genomic circuitry of human disease loci by integrative epigenomics. Nature *590*, 300–307. 10.1038/s41586-020-03145-z.

26. Trimm, E., and Red-Horse, K. (2023). Vascular endothelial cell development and diversity. Nat Rev Cardiol *20*, 197–210. 10.1038/s41569-022-00770-1.

27. Liu, S., Gao, W., Ning, Y., Zou, X., Zhang, W., Zeng, L., and Liu, J. (2022). Cardiovascular Toxicity With PD-1/PD-L1 Inhibitors in Cancer Patients: A Systematic Review and Meta-Analysis. Front Immunol *13*, 908173. 10.3389/fimmu.2022.908173.

28. D'Antonio, M., Nguyen, J.P., Arthur, T.D., Matsui, H., Donovan, M.K.R., D'Antonio-Chronowska, A., and Frazer, K.A. (2022). In heart failure reactivation of RNA-binding proteins is associated with the expression of 1,523 fetal-specific isoforms. PLoS Comput Biol *18*, e1009918. 10.1371/journal.pcbi.1009918.

29. Dobin, A., Davis, C.A., Schlesinger, F., Drenkow, J., Zaleski, C., Jha, S., Batut, P., Chaisson, M., and Gingeras, T.R. (2013). STAR: ultrafast universal RNA-seq aligner. Bioinformatics *29*, 15–21. 10.1093/bioinformatics/bts635.

30. Tarasov, A., Vilella, A.J., Cuppen, E., Nijman, I.J., and Prins, P. (2015). Sambamba: fast processing of NGS alignment formats. Bioinformatics *31*, 2032–2034. 10.1093/bioinformatics/btv098.

31. Tischler, G., and Leonard, S. (2014). biobambam: tools for read pair collation based algorithms on BAM files. Source Code Biol Med *9*, 13. 10.1186/1751-0473-9-13.

32. Li, B., and Dewey, C.N. (2011). RSEM: accurate transcript quantification from RNA-Seq data with or without a reference genome. BMC Bioinformatics *12*, 323. 10.1186/1471-2105-12-323.

33. Li, H., Handsaker, B., Wysoker, A., Fennell, T., Ruan, J., Homer, N., Marth, G., Abecasis, G., Durbin, R., and 1000 Genome Project Data Processing Subgroup (2009). The Sequence Alignment/Map format and SAMtools. Bioinformatics *25*, 2078–2079. 10.1093/bioinformatics/btp352.

34. Quinlan, A.R., and Hall, I.M. (2010). BEDTools: a flexible suite of utilities for comparing genomic features. Bioinformatics *26*, 841–842. 10.1093/bioinformatics/btq033.

35. Love, M.I., Huber, W., and Anders, S. (2014). Moderated estimation of fold change and dispersion for RNA-seq data with DESeq2. Genome Biol *15*, 550. 10.1186/s13059-014-0550-8.

36. Satija, R., Farrell, J.A., Gennert, D., Schier, A.F., and Regev, A. (2015). Spatial reconstruction of single-cell gene expression data. Nat Biotechnol *33*, 495–502. 10.1038/nbt.3192.

37. Zhang, Y., Liu, T., Meyer, C.A., Eeckhoute, J., Johnson, D.S., Bernstein, B.E., Nusbaum, C., Myers, R.M., Brown, M., Li, W., et al. (2008). Model-based Analysis of ChIP-Seq (MACS). Genome Biol *9*, R137. 10.1186/gb-2008-9-9-r137.

38. Liao, Y., Smyth, G.K., and Shi, W. (2014). featureCounts: an efficient general purpose program for assigning sequence reads to genomic features. Bioinformatics *30*, 923–930. 10.1093/bioinformatics/btt656.